Available online at www.sciencedirect.com
ScienceDirect
Carbohydrate Research 342 (2007) 1210–1222
Carbohydrate RESEARCH

Octa-*O*-propanoyl-β-maltose: crystal structure, acyl stacking, related structures, and conformational analysis

Glenn P. Johnson,[a] Edwin D. Stevens[b,*] and Alfred D. French[a,*]

[a]*Southern Regional Research Center, US Department of Agriculture, 1100 Robert E. Lee Blvd., New Orleans, LA 70124, United States*
[b]*Department of Chemistry, University of New Orleans, LA 70148, United States*

Received 9 November 2006; received in revised form 21 February 2007; accepted 22 February 2007
Available online 1 March 2007

Abstract—The crystal structure of β-maltose octapropanoate (**1**) was solved to improve understanding of di-, oligo-, and polysaccharide conformations. The O6 and O6′ atoms are in *gg* and *gt* orientations, respectively. Extrapolation of the coordinates of the non-reducing residue and observed linkage bond and torsion angles of **1** ($\tau_{C1'-O4-C4} = 116.0°$, $\phi_{O5'-C1'-O4-C4} = 77.1°$, $\psi_{C5-C4-O4-C1'} = -157.5°$) yields a left-handed helix similar to amylose triacetate I. The ϕ and ψ values of **1** are also similar to those of other crystalline, acylated maltose compounds as well as some hydroxyl-bearing molecules. Acylated maltose moieties are often stabilized by stacking of the carbonyl groups and α-carbons on O3 and O2′ as well as by the *exo*-anomeric effect. The conformation of **1** is within the 1-kcal/mol contour on a hybrid energy map built with a dielectric constant of 7.5, but corresponds to higher energies on maps made with lower dielectric constants. In one region of ϕ,ψ space, both hydroxyl-bearing and derivatized maltose moieties are found but no inter-residue, intramolecular hydrogen-bonding occurs. In another region, only hydroxyl-bearing molecules crystallize and O2′···O3 hydrogen bonds are always found. In agreement with the energy surfaces, amylose helices extrapolated from available linkage geometries were almost all left-handed.

Keywords: Carbohydrate; Conformation; Hybrid; Molecular; Quantum mechanics; Starch; Propionate

1. Introduction

In 1954, Dexter French, father of one of the present authors, published the unit cell dimensions and space group of β-maltose octapropanoate (then called octapropionate) (**1**),[1] but the details of the molecular structure remained undiscovered. Because maltose is the shortest chain of glucose residues that incorporates the α-(1→4) linkage found in starch, a full structure determination was of interest to us because it could give additional experimental information on the range of likely shapes of amylose and amylopectin. It could also elucidate general factors that determine the shapes of carbohydrates. Knowledge of molecular shapes is especially critical for understanding the properties of oligo- and polysaccharides. Practical properties such as viscosity are consequences of the molecular shape, and solid state properties are consequences of the manner in which the individual molecules aggregate to make larger structures. Knowledge-based improvements of performance properties depend on a thorough understanding of structural properties and subsequent utilization of that understanding.

The present article reports the crystal and molecular structure of **1** and compares its features with those of related molecules such as β-maltose octaacetate (**2**), solved in 1982 by Brisse et al.[2] Three acylated cyclomaltoheptaose (β-cyclodextrin, β-CD) molecules[3] are also of particular interest but review of those molecules led to an accompanying paper.[4] Comparisons with the other molecules are done in the context of positions in ϕ,ψ space and potential energy calculations.[5] In addition, we have extrapolated from the geometries of **1** and other small molecules in the literature to predict

* Corresponding authors. Tel.: +1 504 2806856 (E.D.S.); +1 504 2864410; fax: +1 504 2864419 (A.D.F.); e-mail addresses: estevens@uno.edu; afrench@srrc.ars.usda.gov

0008-6215/$ - see front matter © 2007 Elsevier Ltd. All rights reserved.
doi:10.1016/j.carres.2007.02.029

the range of shapes that amylose molecules might take. During our studies, we found that some of the propanoate substituent groups were unexpectedly close to each other. We propose that this 'acyl stacking' can further stabilize conformations that are already benefitting from the *exo*-anomeric effect.[6]

2. Results and discussion

2.1. Crystal and molecular structure details

2.1.1. General. Details of the structure determination are given in Table 1. The unit cell dimensions are essentially the same as those from the 1954 work. The thermal ellipsoid plot with atom numbering is shown in Figure 1. The glucose rings have the usual $^4C_1$ conformation, with puckering parameters[7] of Q, $\theta(2)$, and $\phi(2)$ for the reducing[†] β-D-glucopyranose ring of 0.585 Å, 3.02°, and 11.94°. For the non-reducing α-D-glucopyranose ring, they are 0.513 Å, 4.20°, and 91.41°, respectively. An ideal $^4C_1$ ring would have $\theta(2) = 0.0°$, so both rings are close to being perfect chairs. Given these low values of $\theta(2)$, the values of $\phi(2)$ are fairly unimportant. The reducing ring has a puckering amplitude (Q) in the mid-upper range while Q for the non-reducing ring is low, indicating a somewhat flattened ring. The O4···O4′ distance of the non-reducing ring is 4.421 Å, very close to an average for α-glucose rings of 4.444 Å. The reducing ring's O1···O4 distance is 5.463 Å, average for β-D-glucose residues. The twist of the non-reducing ring, defined by O4′–C4′···C1′–O4, is −6.2°, very near the average value of −6.1°. As seen in the accompanying paper on cyclodextrins,[4] this twist is a variable of special interest in understanding the shapes of cyclodextrins. Being negative, the twist in **1** would confer a bias toward left-handed structures if incorporated in model amylose helices.

The inter-residue glycosidic linkage conforms to the *exo*-anomeric effect,[6] having a torsion angle $\phi_{O5'-C1'-O4-C4} = 77.1°$, while $\psi_{C5-C4-O4-C1'} = -157.5°$ ($\phi_{H1'-C1'-O4-C4} = -35.1°$, $\psi_{H4-C4-O4-C1'} = -34.8°$). The similarity with **2** ($\phi_{O5'-C1'-O4-C4} = 84.2°$, $\psi_{C5-C4-O4-C1'} = -154.8°$) is underscored by a root mean square (rms) deviation of 0.16 Å between the ring and glycosidic linkage atoms of **1** and **2**. The O6 and O6′ atoms have *gg* and *gt* conformations ($\chi_{O5-C5-C6-O6} = -63.9°$ and $\chi'_{O5'-C5'-C6'-O6'} = 61.7°$), respectively. In **2**, O6′ has dual occupancy of the *gt* and *tg* positions, but the small value of the largest difference peak (0.202 electrons per Å^3, Table 1) indicates that there is no significant occupation of the *tg* orientation in **1** despite large thermal motion of O6′. The distribution of O6 atoms is also *gg*, *gt* in two other mostly acetylated derivatives of maltose: 1,6-anhydro-β-maltotriose nonaacetate[8] and β-maltosyl-nitromethane heptaacetate.[9] In 6^{III}-bromo-6^{III}-deoxy-1,6-anhydro-β-maltotriose octaacetate,[8] O6′ and Br are *gg* and *gt*, respectively, as well.

Table 1. Crystal data and structure refinement for maltose octapropanoate

Empirical formula	$C_{36}H_{54}O_{19}$
Formula weight	790.79
Temperature (K)	189(2)
Wavelength (Å)	0.71073
Crystal system, space group	Orthorhombic, $P2_12_12_1$
Unit cell dimensions	
a (Å)	10.0375(6)
b (Å)	17.1713(10)
c (Å)	23.6194(14)
Volume (Å^3)	4071.0(4)
Z, Calculated density (Mg/m^3)	4, 1.290
Absorption coefficient (mm^{-1})	0.105
$F(000)$	1688
Crystal size (mm)	$0.15 \times 0.25 \times 0.5$
θ Range for data collection	1.72–23.26°
Limiting indices	$-11 \leqslant h \leqslant 11$, $-19 \leqslant k \leqslant 19$, $-26 \leqslant l \leqslant 26$
Reflections collected/ unique [$R_{(int)}$]	39,593/5859 [0.0728]
Completeness to θ	23.26 100.0%
Absorption correction	Empirical
Maximum and minimum transmission	1.000000 and 0.759511
Refinement method	Full-matrix least-squares on F^2
Data/restraints/parameters	5859/467/552
Goodness-of-fit on F^2	1.012
Final R indices [$I > 2\sigma(I)$]	$R_1 = 0.0482$, $wR_2 = 0.0971$
R indices (all data)	$R_1 = 0.0985$, $wR_2 = 0.1039$
Absolute structure parameter	0.5(13)
Largest difference in peak and hole (e Å^{-3})	0.202 and −0.216

In **1**, the carbonyl carbon (C7) attached to the reducing oxygen atom eclipses the hydrogen on C1 (H1–C1–O1–C7 = 2.5°, O5–C1–O1–C7 = −119.1°), similar to the other propanoyl groups (see below), and does not conform to the *exo*-anomeric effect. Its orientation is, however, stabilized by a C1–H1···O7 hydrogen bond. In **2** the comparable torsion angles are 46.4° and −76.4°, in better conformity with the *exo*-anomeric effect. Figure 2 shows the energies for the possible orientations at C1 for a model based on acetylated tetrahydropyran; both the 2.5° and 46.4° conformations are in the same flat, low-energy basin.

2.1.2. Propanoyl groups and acyl stacking. As indicated in Figure 1 by the large ellipsoids, there is extensive thermal motion of the propanoyl groups on C1, C6, and C6′. Especially large motions are derived for the terminal carbon atoms C9, C18, and C30, with substantial motion for the corresponding carbonyl oxygen atoms O7, O16, and O28 as well. The propanoyl groups with

[†] The terms 'reducing' and 'non-reducing' refer to the maltose molecule before addition of the propanoyl groups.

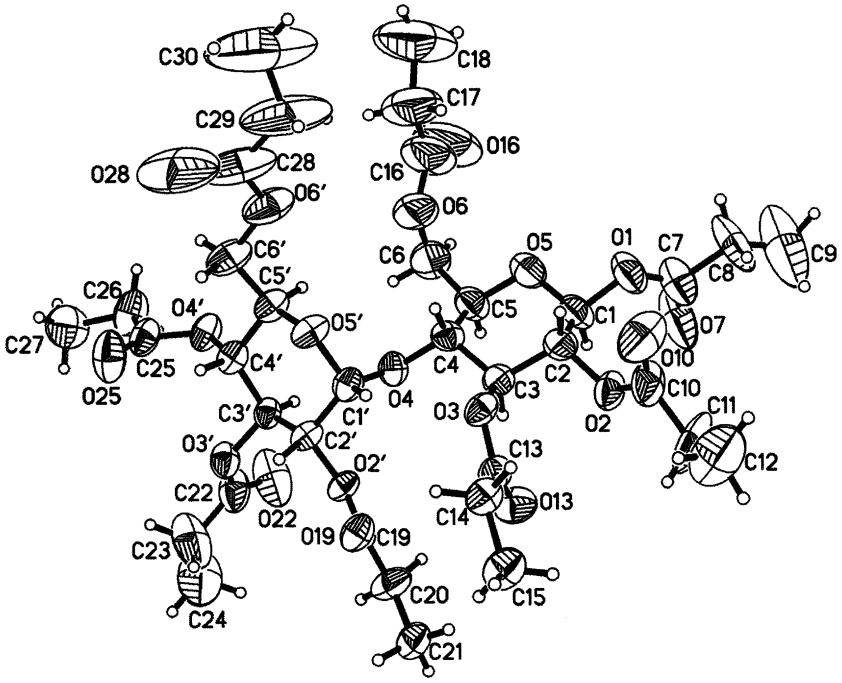

Figure 1. Thermal ellipsoids and atom numbering for maltose octapropanoate. The ellipsoids indicate the regions within which the probability of finding the nuclei is 50%.

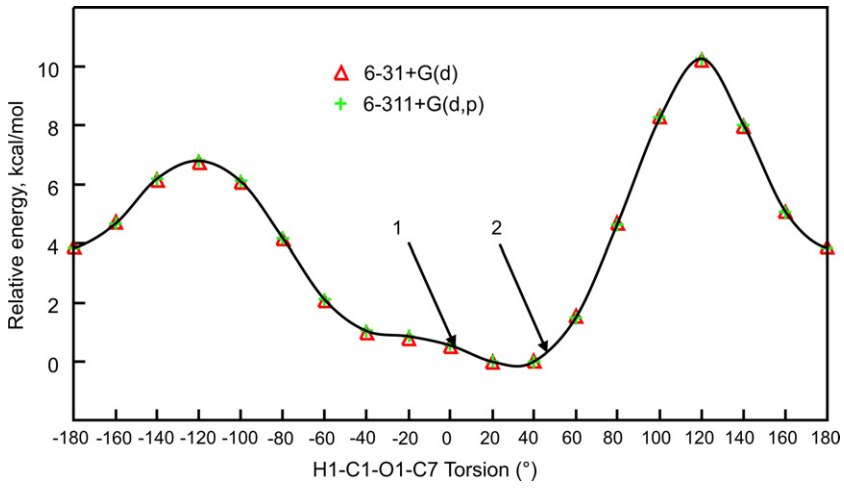

Figure 2. B3LYP/6-31+G(d) and B3LYP/6-311+G(d) energies for various orientations of an 'anomeric' acetate group on tetrahydropyran in an equatorial disposition. Both observed orientations in **1** and **2** with H1–C1–O1–C7 = 2.5° and 46.4°, respectively, have low energies.

the least thermal motion, on C3 and C2′, are in close contact with each other (Fig. 3), even though the O3 and O2′ atoms are well separated (4.04 Å). The close contact suggests that stabilization is arising from 'acyl stacking'.

The phrase 'acyl stacking' has been used previously. In an NMR study of phosphatidylcholines, Arora and Gupta[10] found that the conformation of the glycerol backbone was influenced by vicinal acyl chains. However, their acyl groups were fatty acids that contained 13, 15, or 17 carbons, and their stacking consisted of van der Waals interactions of these long hydrocarbon chains that have parallel alignments. There was no discussion of electrostatic interactions of the carbonyl groups with each other. Of course, dipole–dipole stabilization of carbonyl groups is well known. The molecule 2-bromocyclohexanone forms stacked clusters, the size of which depends on the concentration and dielectric constant of the solvent,[11] and acetone dimers occur in the vapor phase.[12]

Allen et al.[13] found that 15% of all crystals of compounds that contain carbonyl groups have non-bonded

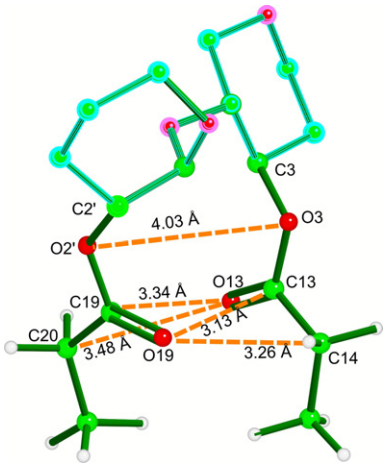

Figure 3. The experimental geometry of maltose octapropanoate, showing just the two rings, the propanoyl groups located on C3 and C2′, and the distances between several pairs of atoms. The short distances indicate attraction between the propanoyl groups despite a fairly long distance between O3 and O2′.

C···O distances of less than 3.6 Å between carbonyl groups. They identified three interaction motifs, including a 'slightly sheared antiparallel' arrangement similar to the one found here. Decomposition of their Inter-Molecular Perturbative Theory (IMPT) quantum mechanics (QM) energies for acetone dimers showed that electrostatics are the primary source of stabilization. However, Allen et al. did not report the additional short distance from the carbonyl oxygen atoms to the α-carbon atoms (C14 and C20 in Fig. 3) that we have found.

Table 2. Intermolecular dipole–dipole interactions (>0.12 kcal/mol) for an MM4-optimized model based on two methyl acetate molecules, numbered according to **1** (dielectric constant of 1.5)

Bond 1	μ1 (Debye)	Bond 2	μ2 (Debye)	$r_{1,2}$ (Å)	E (kcal/mol)
C19–O19	2.000	C13–O13	2.000	3.2467	−0.6862
C19–O19	2.000	C13–C14	−0.925	3.2549	−0.4581
C19–C20	−0.925	C13–O13	2.000	3.2549	−0.4581

Using two methyl acetate molecules derived from the propanoyl groups at C3 and C2′, our MM4[14] empirical force field calculation confirmed (Table 2) that substantial dipole–dipole attractions occur. Besides interactions between the dipoles arising from the C=O bonds, those dipoles also interact with dipoles for the carbonyl carbons and their adjacent α-carbon atoms. These attractive interactions lead to the short interatomic distances shown in Table 3 for **1** and related experimental crystal structures.

Table 3 also shows interatomic distances calculated with B3LYP/6-31G(d) QM, and with both MM4 and the older MM3(96) program.[15] Also in Table 3 are the standard MM4 van der Waals sums for the four given atom pairs. The extent of compression caused by the attractive dipole–dipole and other interactions is indicated by comparing that 14.84 Å total with the 13.04 Å total in the MM4 results that used a dielectric constant of 1.5. Thus, the average distance between these atom pairs is shorter than the sum of the van der Waals radii by 0.45 Å (1.80 Å/4). The sum of the experimental distances for **1** is smaller than for **2**, but larger than for 1,6-anhydro-6^{III}-bromo-6^{III}-deoxy-β-maltotriose octaacetate. The QM and MM4 calculations confirm the short experimental distances, while MM3(96) calculations gave larger distances. Both MM3 and MM4 gave larger distances when the dielectric constant was increased. That, along with the dipole–dipole energies in Table 2, indicates an electrostatic basis for the attraction.

The overall MM4 interaction energy for the two methyl acetates, that is, the energy of the dimer minus twice the energy of a single, isolated methyl acetate

Table 3. Stacking distances for carbonyl groups in crystals and methyl acetate dimer models

Method of determination	Interatomic distances (Å) (see Fig. 3)				
	O13–C19	O19–C13	O13–C20	O19–C14	Total
X-ray experiments					
Maltose octapropanoate (**1**)	3.34	3.13	3.48	3.26	13.21
Maltose octaacetate (**2**)	3.29	3.5	3.33	3.58	13.70
1,6-Anhydromaltotriose nonaacetate	3.17	3.24	3.29	3.30	13.00
1,6-Anhydro-6^{III}-bromo-6^{III}-deoxy-maltotriose octaacetate	3.09	3.13	3.18	3.21	12.61
β-Maltosyl nitromethane heptaacetate	3.44	3.66	3.32	3.74	14.16
Calculations (on methyl acetate dimers)					
Quantum B3LYP/6-31G(d)	3.43	3.43	3.41	3.41	13.68
MM4 1.5	3.29	3.29	3.23	3.23	13.04
MM4 3.5	3.44	3.44	3.36	3.36	13.60
MM4 7.5	3.54	3.54	3.44	3.44	13.96
MM4 van der Waals radii	*3.70*	*3.70*	*3.72*	*3.72*	*14.84*
MM3(96) 1.5	3.67	3.67	3.53	3.53	14.40
MM3(96) 3.5	3.80	3.90	3.69	3.68	15.07
MM3(96) 7.5	3.96	4.03	3.79	3.78	15.56

group, was 3.66 kcal/mol. The dielectric constant was 1.5 in that calculation. We also obtained energies by QM. In the above B3LYP/6-31G(d) calculations, the dimerization energy was −4.27 kcal/mol. That larger QM value may be an overestimation because of Basis Set Superposition Error (BSSE). BSSE is a problem with that basis set and method in dimerization energies for hydrogen-bonded water.[16] Minimization calculations with B3LYP/6-311+G(d), which should avoid most BSSE, gave −2.41 kcal/mol. In that calculation, however, there were substantial changes in the structure, with an increase in distance between the non-bonded carbonyl oxygen and carbon atoms, and formation of a C–H···O hydrogen bond. We also determined the energy of interaction by calculating the energy for four compounds: (1) an analog of maltose that lacked any substituents except C6 and C6′ methyl groups; (2) and (3) the same molecule with an acetate group in the 3 or 2′ position and (4) the same compound with both substituents. The sum of the energies of adding each substituent was compared with the energy of adding both groups, at several levels of theory. Energies ranged from −1.7 to −2.9 kcal/mol. Again, more complete basis sets with diffuse functions and the B3LYP method resulted in geometry changes of the acyl–acyl interaction.

Sparks et al.[17] calculated QM dimerization energies for acetone and obtained −1.5 to −3.4 kcal with various density functional theory methods, and −4.4 kcal with MP2, all with the 6-311+G(d,p) basis set. Those values are less stabilizing than the −5.3 kcal found with the IMPT calculations of Allen et al. for the 'slightly sheared antiparallel' motif. Other workers[18] have found that calculating the dimerization energy of even formaldehyde is complex. In view of that, and the different motifs,[13] we decided that a more precise result for acyl groups would require a separate project.

We also looked at crystalline acetylated trehalose and sucrose in the Cambridge Structural Database (CSD).[19] Neither of those sugars had inter-residue acyl stacking, but the two sucrose derivatives in the RASSOU structure[20] and nine trehalose molecules exhibited short, non-bonded distances between the carbonyl carbon and oxygen atoms of vicinal acetate groups. In those intra-residue interactions, a number of the distances between the carbonyl oxygen and α-carbon atoms were longer than 3.7 Å. Thus, there is a fair amount of variation in the exact details of acyl–acyl interactions, even in acylated carbohydrates. The defining characteristic of acyl stacking should be a roughly antiparallel arrangement of carbonyl bonds that places the respective atoms in closer distances than would be expected based on the van der Waals radii. Interactions may be stronger if the carbonyl carbon to α-carbon atom dipole is also involved. In the following paper,[4] we report the stacking of three acyl groups.

The H*n*–C*n*–O*n*–C*x* torsion angles (where *n* is 1, 2, 3′, and 4′ and *x* is 7, 10, 22, and 25, respectively) are nearly eclipsed, at 2.5°, −0.3°, 12.0°, and −8.8°. For the propanoyl groups on C3 and C2′ involved in the stacking, the torsions are 20.1° and −33.1°. These larger deviations from the apparently preferred[21] value of 0° allow the group on C3 to move closer to the group on C2′, whereas the rotation of the C2′ group better aligns it with the group on C3. All of the conformations involving the former secondary hydroxyl groups are stabilized by C–H···O hydrogen bonds with the ring methine hydrogen as the donor and the carbonyl oxygen as the acceptor. The methine hydrogen on C1′ donates to O3, the former hydroxyl oxygen on C3. That inter-residue interaction may also stabilize the ϕ and ψ torsion angles. Only two intermolecular C–H···O hydrogen bonds were found. In one case, H1 is donated to an adjacent O19, and in the other, H26A donates to a nearby O10.

Most of the propanoyl groups have nearly eclipsed O*n*=C*n*–C(*n*+1)–C(*n*+2) torsion angles, where $n = 7$, 10, 13, 16, 19, 22, 25, and 28. The angles are 10.9°, 17.9°, 2.1°, 6.7°, −178.9°, 2.2°, −13.1°, and −40.1°. The *trans* (*anti*) value (−178.9°) is for the group at C2′ that is involved in the stacking interaction. The torsion of −40.1° includes C30, the end of the propanoyl group at C6′ where the thermal motion is greater than for all other atoms except its attached hydrogens (deposited data).

2.1.3. Bond lengths. One expected consequence of large thermal motion is substantial underestimation of the observed bond lengths, with values as small as 1.374(8) Å for the C7–C8 bond (not shown), clearly too short for an sp^3–sp^3 link. On the other hand, the ring and former hydroxyl atoms of the maltose moiety in **1** do not have extreme thermal motion, so distances derived from those atoms should be ordinary. However, when comparing C–C lengths in **1** with individual bond averages from β-maltose monohydrate,[22] and α- and β-glucose,[23,24] the bonds are 0.02 Å shorter. Averaging the lengths in **1** with those in the pentaacetates of α- and β-glucose[25,26] and β-maltosylnitromethane heptaacetate[9] gave a difference of 0.01 Å. Subsequent calculations on acetylated and on unsubstituted α- and β-glucose at the B3LYP/6-311+G(d) level did not confirm that the C–C bonds of **1** should be generally shorter (Fig. 4a), leaving us without an explanation for the experimental observation. The calculations did indicate that the C5–C6 bonds should be shorter than other C–C bonds in the case of structures with O6 in the *gt* position. Also, the calculations (Fig. 4b) showed that C–O bonds leading to the acyl groups should be longer than in the unsubstituted molecule. The C–O lengths were similar to the average values for the comparable bonds in galactose pentaacetate,[21] and in MM4 that type of oxygen atom has suitably longer C–O bonds.

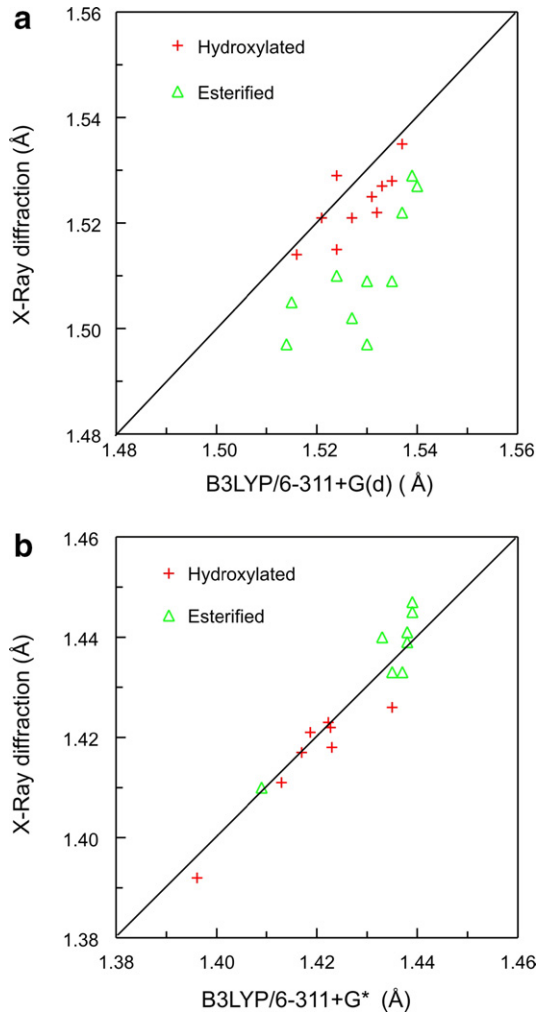

Figure 4. Experimental (a) C–C and (b) C–O bond lengths from **1** (esterified), averaged with data from glucose pentaacetates and β-maltosylnitromethane heptaacetate, compared with results from B3LYP/6-311+G(d) calculations. Also shown are bond lengths for the native (hydroxyl-bearing) glucose and maltose molecules. All C–C bonds found in the native molecules were included, while C–O bonds were from those attached to the 1, 2, 3, 6, and 2′, 3′, 4′, and 6′ carbons. The diagonal line shows the ideal, on which all points would fall if there were no differences among the structures or computational methods. The shortest bond lengths in each set in (b) are for the C1–O1 bond in the β-configuration.

2.1.4. Crystal packing. The packing arrangement of **1** projected onto the *b*–*c* plane is shown in Figure 5a. Because of the $P2_12_12_1$ space group, with its three mutually perpendicular, non-intersecting screw axes, the crystal packing is difficult to visualize, a problem exacerbated by the propanoate substituents that fill up most of the gaps in the structure. We found it helpful to delete all hydrogen atoms and the ethane moieties of each propanoate. Although the deleted alkyl groups participate in many of the intermolecular interactions, their deletion leaves channels that are parallel to the unit cell diagonals ([0 1 1] and [0 −1 1]). This allows the periodicity to be more easily visualized, and the channels leave islands that are based on two maltosyl units per unit cell. The C6 groups project into the intersections of the two channels, presumably giving them maximum opportunity for thermal motion.

A closer view of the maltosyl units that are related by the twofold screw-axis that is parallel to the *a*-axis and crosses the *b*-axis at 0.75 is shown in Figure 5b. In this close-up, only the hydrogen atoms were eliminated. The projections onto both the *b*–*c* plane (left) and onto the *a*–*b* plane (right) include the symbols for the screw-axis. The O3 and O2′ propanoyl groups are closest to that screw-axis, with the ethane parts of the propanoyl groups reaching past the screw-axis toward the related molecule.

2.2. ϕ,ψ Conformation

2.2.1. Comparisons with other experimental work. The work on **2** by Brisse et al.[2] reviewed the conformations of related molecules in the context of a rigid residue energy map. Since then, the number of available maltose linkage geometries from small molecule crystals, not including CDs, has increased nearly fivefold. In addition, more than 2000 linkages have now been characterized in CDs and variants with more than 10 glucose residues called cycloamyloses (CAs). All of these geometries, including non-macrocyclic linkages, have been plotted on energy maps for several molecules, including perfluorinated maltose,[27] but no detailed analysis was carried out. The CD and CA linkages have a wide range of ϕ and ψ values, including a presence in an otherwise unoccupied secondary minimum. That shows the flexibility of the α-1,4 linkage, but the macrocycle may cause some strain that would not be found in the non-macrocyclic structures. We have worked toward resolving that issue in the accompanying paper.[4] Other linkage geometries are available from crystalline complexes of proteins with maltose and its oligomers,[28] but such structures are less accurate and again, extra strain is likely in at least some examples. Herein, we will discuss only non-macrocyclic structures. Their citations and full compound names are given in Table 4 along with their Cambridge Structural Database Refcodes.

The locations of the 36 available linkage geometries from non-macrocyclic structures are shown in Figure 6. Both ϕ and ψ values have ranges of more than 60°, with the range of ψ values being largest when ψ_H is about −10°. Conformations from the 10 unique linkages in the *p*-nitrophenol maltohexaoside–iodine complex crystal structure (shown as circles) span almost the entire observed range. The structure closest to **1** is IPMALT (phenyl 6^I-deoxy-6^I-iodo-α-maltoside), a molecule with six of the eight hydroxyl groups that are found on maltose. Its ring and inter-residue linkage oxygen atoms have only a 0.14 Å rms deviation with those of **1**, an even better agreement than between **1** and **2**.

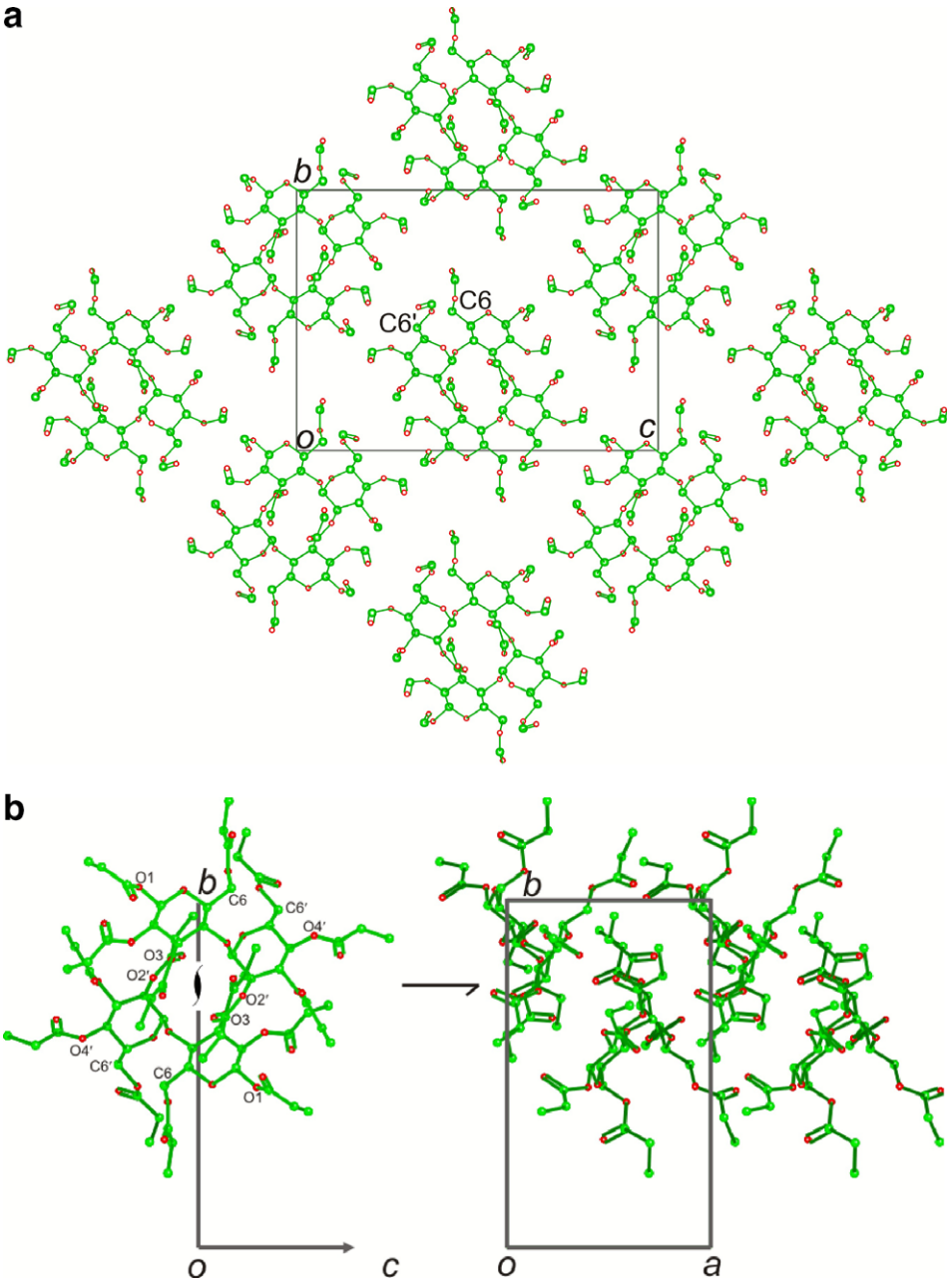

Figure 5. Crystal packing in **1** (see text). (a) Projection onto the *b*–*c* plane with the unit cell shown. C6 and C6′ groups are indicated on one molecule to show their proximity to the intersection of the channels. (b) Left: close-up view of *b*–*c* projection showing the position of the 2_1 screw-axis. Two molecules of **1** are shown. Right: Projection onto the *a*–*b* plane, with four molecules of **1** shown as well as the screw-axis symbol.

A dashed line in Figure 6 separates the structures that lack inter-residue O3···O2′ hydrogen-bonding from those that have it. Conclusions about the presence of hydrogen bonds were based on a donated hydroxyl hydrogen within 2.15 Å of the acceptor oxygen or, when no hydrogen coordinates were available, by an O···O distance <3.05 Å. Below the line, there is a mixture of hydroxyl-bearing structures that form other hydrogen bonds instead of the intramolecular O3···O2′ bond, as well as derivatized structures such as **1** that cannot make conventional hydrogen bonds.

All five fully substituted structures fall in a small region of ϕ,ψ space. The TAQXUE and TAQXOY structures are isomorphous, with essentially identical unit cell dimensions and crystal packing, but the others have completely different crystals. Despite not being isomorphous, the two hydroxyl-bearing DUDXOP linkages, the acetylated WEHTIM and (**2**) are closer in ϕ,ψ space to TAQXUE than TAQXUE is to its isomorphous mate, TAQXOY.

This grouping of molecules that are either hydroxyl-bearing or acylated suggests that the normal conforma-

Table 4. Refcodes and chemical names for compounds related to maltose octapropanoate

CSD Refcode and citation	Chemical name
DUDXOP[40]	Methyl α-maltotrioside tetrahydrate
FOXSUG20[41]	Barium bis(*p*-nitrophenol α-maltohexaoside) bis(tri-iodide) hydrate
HAHXUJ[42]	*O*-β-D-Fructofuranosyl-(1→2)-*O*-α-D-glucopyranosyl-(1→4)-α-D-glucopyranoside monohydrate (erlose monohydrate)
HEGXOG[43]	*O*-β-D-Fructofuranosyl-(1→2)-*O*-α-D-glucopyranosyl-(1→4)-α-D-glucopyranoside (erlose trihydrate)
IPMALT[44]	Phenyl 6^{I}-deoxy-6^{I}-iodo-α-maltoside
KOYZAZ[45]	*O*-α-D-Glucopyranosyl-(1→6)-*O*-α-D-glucopyranosyl-(1→4)-D-glucose (α,β-panose)
MAPNEW[46]	μ_2-(Peroxo)-bis(*N*,*N*′-bis(maltosyl)-tris(2-aminoethyl)amine)-cobalt(III)) trichloride methanol solvate hydrate
MALTOS11[22]	β-Maltose monohydrate
MALTOT[47]	α-Maltose
MENRAY[48]	4-*O*-α-D-Glucopyranosyl-4-*O*-α-D-glucopyranosyl-D-glucitol (maltotritol)
MMALTS[49]	Methyl β-maltoside monohydrate
PHMALT[44]	Phenyl α-maltoside
TAQXOY[8]	1,6-Anhydro-β-maltotriose nonaacetate
TAQXUE[8]	1,6-Anhydro-6^{III}-bromo-6^{III}-deoxy-β-maltotriose octaacetate
WEHTIM[9]	β-Maltosylnitromethane-heptaacetate
ZZZTUC01[3]	β-Maltose octaacetate (**2**)
ZZZRZQ01	Present work, proposed Refcode (**1**)

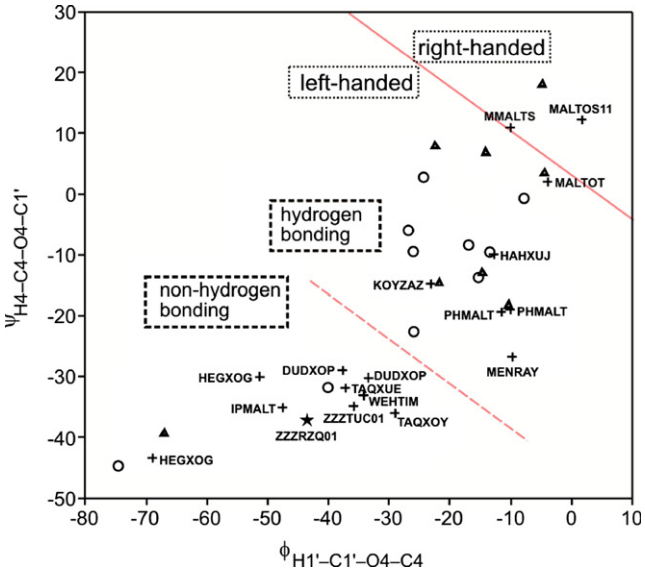

Figure 6. Distribution in ϕ,ψ space for diffraction structures of molecules related to maltose. Points are labeled by their Refcodes from the Cambridge Crystal Structure Data Base (see Table 4 for translation of the Refcodes). The ★ represents the conformation in **1**. Linkage geometries from the FOXSUG20 structure are represented by ○, and those from the MAPNEW structure are indicated by ▲. A dashed diagonal line separates the structures that form an O3–O2′ hydrogen bond from the structures that do not. The solid diagonal line represents polymeric structures having an *h* (advance per residue) of zero. Linkages above the line lead to right-handed helices, while those below lead to left-handed molecules.

tion of the maltose molecule is very similar to **1** if it is not making an O3···O2′ hydrogen bond. That would be the likely situation in dilute aqueous solution, for example. On the other hand, there is a wide range of conformations that can be achieved if assisted by the intramolecular hydrogen bond. This is different from the situation with cellobiose structures. Both maltose and cellobiose give ϕ,ψ distributions with separate regions where inter-residue hydrogen-bonding occurs and where it does not. However, the cellobiose region where hydrogen-bonding occurs also has non-hydrogen-bonded structures,[29] whereas the region for maltose in which hydrogen-bonding occurs has only hydrogen-bonded structures (except for the derivatized CDs, see the accompanying paper).[4]

2.2.2. Comparison of experimental maltosyl structures with energy surfaces. Acyl stacking and the C–H···O hydrogen-bonding between H1′ and O3 are not the only causes for the ϕ and ψ torsion angles of **1**. As mentioned above, the ϕ torsion angle is consistent with the *exo*-anomeric effect that should provide stabilization of the observed conformation. This is confirmed by the location of **1** near the global minima of our potential energy maps for a number of maltose-type molecules that lack hydrogen-bonding ability. These maps include a QM energy surface[30] for a maltose analog composed of two tetrahydropyran rings that were linked with the appropriate 'glycosidic' linkage. Another map was based on permethylated maltose,[31] studied with MM3, and one was calculated for perfluorinated maltose with QM.[27] The conformation of **1** is also near the minimum of an analog map that was first shown in Ref. 27. That same map, made for a maltose analog with two tetrahydropyran rings and methyl groups to represent the C6 and C6′ groups of maltose, is shown in the following paper and discussed in the context of CDs.

Hybrid[32,33] energy surfaces for unsubstituted α-maltose at dielectric constants of 1.5, 3.5, and 7.5 are shown

in Figure 7. All are similar in that there is one central minimum, and a secondary minimum close to the middle of the bottom edge. Figure 7a, made with a dielectric constant of 1.5, has almost all of the hydrogen-bonding geometries from Figure 6 located within the 1-kcal/mol contour and the remaining two are just outside. However, the non-hydrogen-bonding geometries are on one small part on the side of the energy well, with **1** having a corresponding energy of more than 4.0 kcal/mol. Other structures have energies >6 kcal/mol. This positioning of the observed non-hydrogen-bonding structures in a narrow region without any corresponding indication from the energy contour lines could be called the '8 o'clock problem.'

Lower corresponding energies for the non-hydrogen-bonding structures, with an energy less than 2.0 kcal/mol for **1** and a maximum corresponding energy of just over 3.0 kcal/mol are provided in Figure 7b. At the same time, the hydrogen-bonded structures have low energies, similar to those in Figure 7a. While the low-energy contours in Figure 7a are roughly concentric circles, those in Figure 7b are elongated along a diagonal line that would be described approximately by $\psi = \phi$, more in keeping with the experimental geometries.

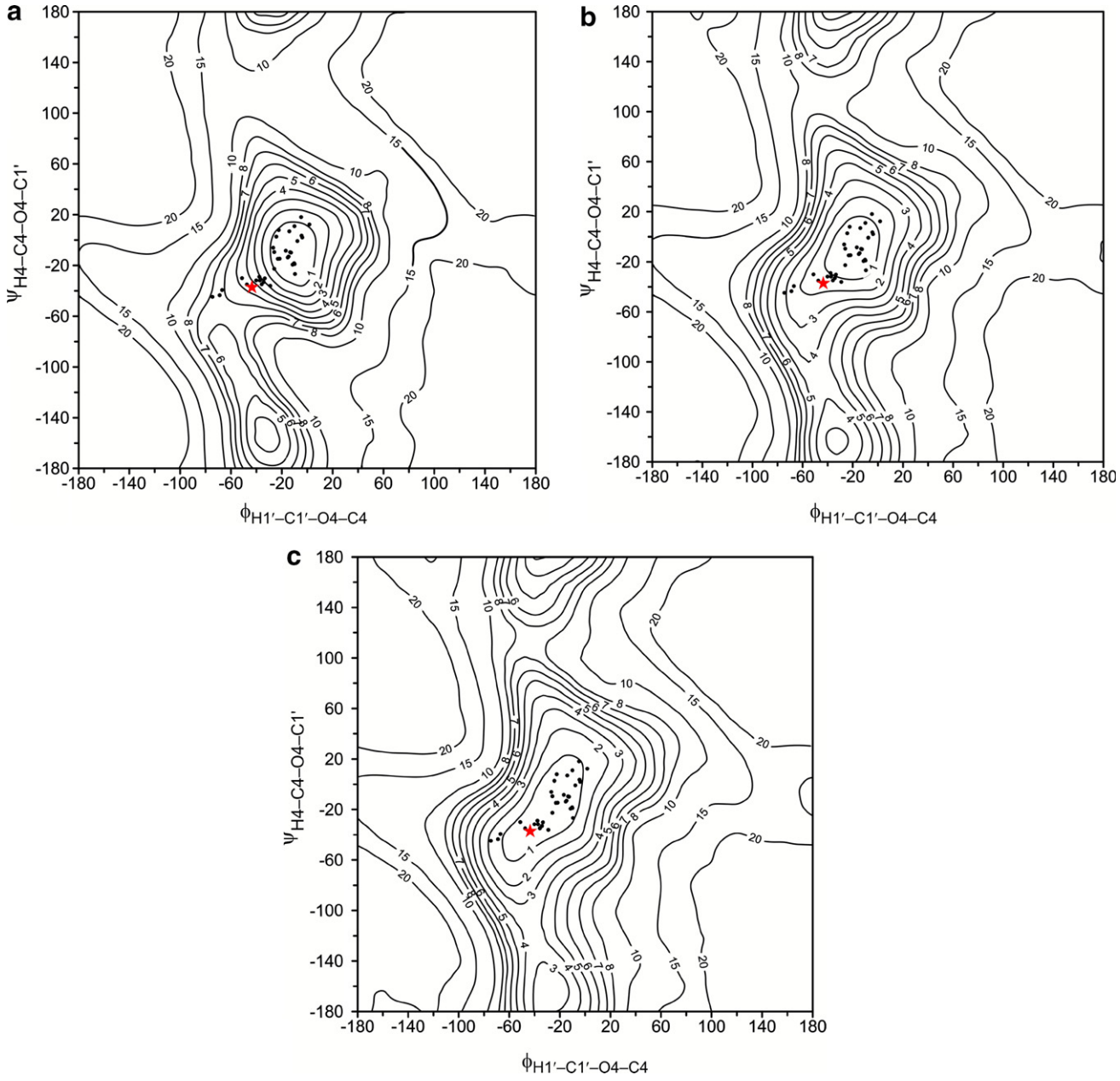

Figure 7. Hybrid (see text) potential energy surfaces for maltose. The ★ represents the linkage conformation observed in **1** and all other conformations from Figure 6 are shown by dots. (a) Dielectric constant set to 1.5. (b) Dielectric constant set to 3.5. (c) Dielectric constant set to 7.5. Contours above 20 kcal/mol are not shown; other contours (9, 11–14, 16–19) are omitted to avoid clutter.

Figure 7c places almost all experimental structures from small molecules inside the 1.0 kcal/mol contour. We consider this surface as the most predictive, in that all of the observed structures have low-energy and all of the low-energy space is populated. This is in strong contrast to 7a, where there are corresponding energies >6 kcal/mol, but only a small portion of the space between the 1- and 5-kcal/mol contours is occupied. On all three surfaces, the MALTOS11 structure corresponds to just over 1.0 kcal/mol.

2.3. Extrapolation to helical amylose

One major reason for studying di- and oligosaccharides that can be precisely determined is to learn their implications for related larger molecules that are usually more difficult to study. The idea is that geometries found in small molecules should be especially likely for larger molecules. The descriptors of a particular disaccharide shape (e.g., ϕ and ψ) do not, however, readily convey a picture of the shape of a polymer. If a polymer such as amylose has a structure wherein all residues and linkage geometries are identical to every other, it will be a helix in the mathematical sense, with screw-axis symmetry. The shape of the polymer that incorporates disaccharide geometry can then be described in terms of helix parameters,[34] so the task at hand is to utilize the small molecule geometries from the different structures in helix fragments and then determine the parameters.

With molecular graphics software, it is simple to connect three copies of a particular glucose ring with a specific linkage geometry, all obtained, for example, from a crystal structure study. The positions of the four linkage oxygen atoms of such a trisaccharide fragment of a helix constitute the necessary information to determine the helix parameters r, n, and h. Here, r represents the radius of a helical thread that passes through the O4 atoms; n is the number of glucose residues per helix turn; and h is the advance (or rise) per residue along the helix axis. By convention, left-handed helices have negative values of n. We have incorporated the equations worked out by Shimanouchi and Mizushima[35] in a spreadsheet[29] for determining these helical parameters. Because no energies are calculated, the method does not identify helix models with low values of h that would have the self-intersection or 'excluded volume' problem. As a guide, when values of the product of $n \times h$ are much less than 8 Å, self-intersection of long polymers will occur; short sequences with $h \approx 0$ are candidates for toroidal (doughnut-shaped) CD structures.

The extrapolated model amylose tripropanoate helix based on the non-reducing residue of **1** has $n = -4.63$ and $h = 3.99$ Å, and values are -4.66 and 3.49 Å for **2**. Those n values are essentially the same as -4.67, the experimentally proposed value for amylose triacetate (ATA) I,[36] while the modeled h values bracket the ATA I X-ray value of 3.85 Å. The ATA I helix proposed from experimental fiber diffraction studies has a backbone of 14 identical glucose rings that make three helix turns in one repeat. That description might seem inconsistent with the reported $P2_12_12_1$ space group. However, the acetate groups of ATA I do not all possess the same orientations, so the actual asymmetric repeating unit has seven acetylated glucose residues that generate 1.5 helix turns. In that repeating unit, we found two strong examples of inter-residue acyl stacking and a good example of intra-residue stacking, besides one weaker example of each. This is despite linkage conformations that are all

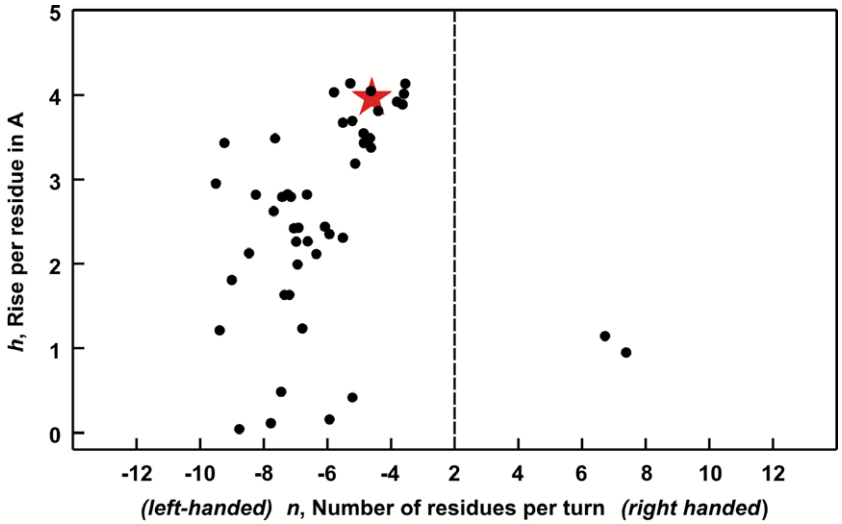

Figure 8. An n–h map for amylose, showing the conformations for the various extrapolated amylose helices. The extrapolated n–h point for **1** is indicated by the ★. The vertical dashed line separates left- and right-handed structures. Structures with $h = 0$ or with $n = 2$ are neither right- nor left-handed.

nearly identical to those in our extrapolated model of amylose tripropanoate, which would have inter-residue acyl stacking at every linkage.

An *n*–*h* map[29,37] for model amylose helices that were constructed in a similar manner but based on all of the structures in Table 4 is shown in Figure 8. Distances from the helix center to the thread that connects the linkage oxygen atoms (*r*, not shown) range from 1.10 to 6.6 Å. There is an almost continuous occurrence of extrapolated model helices on the left-hand side, but only two crystal structures led to right-handed structures: MALTOS11 (with $n = 7.39$ and $h = 0.95$ Å) and one of the MAPNEW structures ($n = 6.73$ and $h = 1.15$ Å). The left-handed model helices in Figure 8 have values of *n* ranging from −3.55 (FOXSUG20) to −9.50 (MAPNEW), with *h* values of 0.04 Å (MMALTS) to 4.13 Å (FOXSUG20). The average of all left-handed *n* values is −6.1 and the average *h* is 2.48 Å, but description of the amylose helix conformation with averages masks its extensive flexibility.

The ϕ,ψ points for the two right-handed molecules are above the solid line of Figure 6 that indicates ϕ,ψ combinations that lead to $h = 0$, that is, they are neither right- nor left-handed. This line, with $\psi_H \approx -\phi_H$, was calculated with the spreadsheet mentioned above and the MALTOS11 structure for all combinations of ϕ and ψ. (Only the $h = 0$ line is shown.) The MMALTS structure is shown as just barely on the right-handed side of the line in Figure 6, as determined from just its ϕ and ψ values. However, its helical parameters, when calculated from its own atomic coordinates and glycosidic bond angle, are $n = -8.77$ and $h = 0.04$ Å, that is, a slightly left-handed structure. Therefore, although Figure 6 shows that three structures lead to right-handed helices, only two right-handed models are indicated in Figure 8.

Although there is little energy cost for a disaccharide to switch between left- and right-handed structures via structures with $h = 0$, longer molecules would have a self-intersection problem. An alternative path for transitions between left- and right-handed amylose helices where $n = 2$ is provided in Figure 8. Although such helices are not forecast in Figure 8, geometries from the flipping regions of the CAs[38] such as CA26[39] do lead to 2-fold, very extended structures. Figure 8 is based only on the molecules listed in Table 4. Regardless of whether the $h = 0$ or the $n = 2$ pathway would be used to convert from left- to right-handed, the energy surfaces in Figure 7 do not provide much low-energy area for structures above the $\psi_H \approx -\phi_H$ line, that is, for right-handed structures.

3. Conclusions

We have solved the crystal structure of maltose octapropanoate and then taken advantage of the new geometric data as well as literature data to learn more about the factors that determine the shape of carbohydrates, especially polysaccharides. With simple models that involve only geometric manipulations of experimentally determined glucose rings, we proposed a range of possible shapes for amylose helices. We also used molecular modeling based on sophisticated empirical force fields and electronic structure theory to confirm our experimental findings. Stacking of acyl groups seems to play a significant, if not dominant, role in determining the relative stabilities of conformers of acylated carbohydrate derivatives. One unresolved issue was our failure to confirm the experimental findings of short C–C bonds in the glucose rings, although the C–O bond lengths were very well predicted.

The maltose moiety of our new structure (**1**) has a shape similar to several acetylated small molecules and it is also similar to some hydroxyl-bearing maltose moieties that do not make the classic O3···O2′ hydrogen bond. Those structures are in a part of ϕ,ψ conformation space that is separate from the region where structures do make the intramolecular hydrogen bond. That hydrogen-bonding domain contains no substituted maltose-like structures with the exception of derivatized CDs (see the following paper). In analogous studies of cellobiose, structures incapable of making hydrogen bonds adopt the same ϕ,ψ conformations as those that can, and vice versa. It would be interesting to have crystal structures of other extensively substituted maltose derivatives to see whether this finding persists.

Electrostatic interactions were important in two somewhat contradictory ways. On the one hand, there is an attractive, dipole–dipole interaction between the propanoyl groups on C3 and C2′ that is made by all five available esterified maltosyl structures. Lowered strength of the electrostatic interactions through a raised dielectric constant in the modeling calculations increased the distance between the two propanoyl groups beyond the observed values. On the other hand, use of full strength electrostatics, and hence full strength hydrogen-bonding, made our hybrid energy surface for maltose unable to predict the structures that do not contain the O3···O2′ hydrogen bond. Cutting the strength of the electrostatics to 20% of the full strength by increasing the dielectric constant to 7.5 (compared to 1.5, the default value for isolated molecules in MM3 and MM4) enabled our mapping procedure to account for all of the observed structures, not just the ones having hydrogen bonds.

Finally, predictions of amylose helices from a large number of experimental geometries is an advance over earlier work that was either limited to one geometry or assumed that it was reasonable to combine ring shapes and linkage geometries from different sources. With the larger number of rings and associated linkages now available, it was possible to predict the range of

amylose shapes based on individual ring shapes and their associated linkage geometries. A nearly continuous range of amylose shapes having between 3.5 and 9.5 residues per turn was indicated. Further, the helices could be compressed (some h values were almost 0) or extended to the point that the h values were as large as distances between O1 and O4 for some of the other experimentally measured glucose residues.

4. Experimental

A single crystal suitable for data collection was mounted on a Bruker SMART single crystal X-ray diffractometer with a 1 K CCD detector. The crystal was cooled to 150(2) K in a stream of cold nitrogen gas, and X-ray diffraction data were collected using Mo Kα radiation. Unit cell dimensions were obtained by least-squares refinement of positions of 5859 observations in the range $1.72° < 2\theta < 23.26°$. The structure was solved by direct methods and optimized by full-matrix least-squares refinement of F^2 including all observations $>2(\sigma)$. All hydrogen atoms were located in a difference Fourier synthesis and included in the least-squares refinement with isotropic thermal parameters.

The locations of 12 hydrogen atoms were obtained from a difference Fourier synthesis and included in the least-squares refinement with isotropic temperature factors. The remaining hydrogen atoms were included in the refinement at calculated positions, and allowed to ride on the carbon atoms to which they were bonded. For methyl hydrogens, idealized tetrahedral geometry was maintained, and the torsional orientation about the C–C bond for each methyl group was included as a parameter in the refinement.

5. Calculations

Calculations were carried out on our multi-processor compute farm under the Linux operating system. Quantum mechanics calculations were performed with Jaguar 5.5, Schrodinger, LLC, Portland, Oregon, and MM3 and MM4 calculations were carried out with the academic versions of the software, obtained from Professor Allinger, University of Georgia. Hybrid energy surfaces were based on maps calculated with MM3(96), modified with the MM3(92) hydrogen-bonding parameters that better reproduce hydrogen bonds in the solid state. There were 58 different combinations of orientations of *exo*-cyclic groups tried at each ϕ,ψ point. A quantum mechanical contribution to the energy surface in our hybrid method is achieved by also calculating energy maps for an analog of maltose based on two tetrahydropyran (THP) rings with the appropriate 'glycosidic' linkage. The THP–O–THP map calculated by MM3 was subtracted from the MM3 map based on the full disaccharide, and the THP–O–THP map calculated by HF/6-31G(d) quantum mechanics was added. An example for maltose is illustrated in Ref. 28. To compensate for the possibility that the hydrogen atoms are not correctly located in diffraction studies, ϕ_H and ψ_H for plotting the experimentally observed conformations were computed from the $\phi_{O5'}$ and ψ_{C5} torsion angles by subtracting and adding, respectively, 120°.

Average values of the twist parameter were calculated from 27 glucose residues taken from the crystal structures in Table 4. Not included were values from the relatively low-resolution FOXSUG20 and MAPNEW structures. The O1···O4 distances for α-glucose were calculated from all the residues from Table 4 that were used to make extrapolated helices. Those for β-glucose were taken from residues used to make extrapolated helices in Ref. 29.

6. Supplementary data

Complete crystallographic data for the structural analysis have been deposited with the Cambridge Crystallographic Data Centre, CCDC No. 626453. Copies of this information may be obtained free of charge from the Director, Cambridge Crystallographic Data Centre, 12 Union Road, Cambridge, CB2 1EZ, UK. (fax: +44-1223-336033, e-mail: deposit@ccdc.cam.ac.uk or via: www.ccdc.cam.ac.uk).

Acknowledgments

The crystal was furnished by Professor J. Robyt, Iowa State University. We thank Dr. J. Vercellotti, V-Labs, Covington, LA, for helpful discussions. Professor N. L. Allinger of the University of Georgia furnished information on the stacking of ketones. Professor T. B. Grindley of Dalhousie University commented on a draft of the manuscript as did Dr. V. Edwards of the Southern Regional Research Center. Dr. M. Mohamed Naseer Ali from the CERMAV called attention to the papers by Allen et al. and Sparkes et al. This work was supported by normal research funding from the Agricultural Research Service, US Department of Agriculture, and was conducted in part as a class project at the University of New Orleans.

References

1. French, D. *Acta Crystallogr.* **1954**, *7*, 136–137.
2. Brisse, F.; Marchessault, S.; Peréz, S.; Zugenmaier, P. *J. Am. Chem. Soc.* **1982**, *104*, 7470–7476.
3. Anibarro, M.; Gessler, K.; Uson, I.; Sheldrick, G. M.; Harata, K.; Uekama, K.; Hirayama, F.; Abe, Y.; Saenger, W. *J. Am. Chem. Soc.* **2001**, *123*, 11854–11862.

4. French, A. D.; Johnson, G. P. *Carbohydr. Res.*, in press, doi:10.1016/j.carres.2007.02.033.
5. Rao, V. S. R.; Qasba, P. K.; Balaji, P. V.; Chandarasekaran, R. *Conformation of Carbohydrates*; Harwood Academic: Amsterdam, 1998, pp 91–130.
6. Tvaroska, T.; Bleha, T. Anomeric and *exo*-anomeric effects in carbohydrate chemistry. *Adv. Carbohydr. Chem. Biochem.* **1989**, *47*, 45–123.
7. Cremer, D.; Pople, J. A. *J. Am. Chem. Soc.* **1975**, *97*, 1354–1358.
8. Kamitori, S.; Itazu, K.; Noguchi, K.; Okuyama, K.; Kitamura, S.; Takeo, K.; Ohno, S. *Carbohydr. Res.* **1995**, *278*, 195–203.
9. Koll, P.; Petrusova, M.; Petrus, L.; Zimmer, B.; Morf, M.; Kopf, J. *Carbohydr. Res.* **1993**, *248*, 37–43.
10. Arora, A.; Gupta, C. M. *Biochim. Biophys. Acta* **1997**, *1324*, 47–60.
11. Allinger, J.; Allinger, N. L. *Tetrahedron* **1958**, *2*, 64–76.
12. Pennington, R. E.; Kobe, K. A. *J. Am. Chem. Soc.* **1957**, *79*, 300–307.
13. Allen, F. H.; Baalham, C. A.; Lommerse, J. P. M.; Raithby, P. R. *Acta Crystallogr., Sect. B* **1998**, *54*, 320–329.
14. (a) Lii, J.-H.; Chen, K.-H.; Allinger, N. L. *J. Comput. Chem.* **2003**, *24*, 1504–1513; (b) Allinger, N. L.; Chen, K.-H.; Lii, J.-H.; Durkin, K. A. *J. Comput. Chem.* **2003**, *24*, 1447–1472; (c) Lii, J.-H.; Chen, K.-H.; Durkin, K. A.; Allinger, N. L. *J. Comput. Chem.* **2003**, *24*, 1473–1489; (d) Lii, J.-H.; Chen, K.-H.; Grindley, T. B.; Allinger, N. L. *J. Comput. Chem.* **2003**, *24*, 1490–1503; (e) Lii, J.-H.; Chen, K.-H.; Allinger, N. L. *J. Comput. Chem.* **2003**, *24*, 1504–1513; (f) Lii, J.-H.; Chen, K.-H.; Johnson, G. P.; French, A. D.; Allinger, N. L. *Carbohydr. Res.* **2005**, *340*, 853–862.
15. (a) Allinger, N. L.; Yuh, Y. H.; Lii, J.-H. *J. Am. Chem. Soc.* **1989**, *111*, 8551–8566; (b) Lii, J.-H.; Allinger, N. L. *J. Am. Chem. Soc* **1989**, *111*, 8566–8575; (c) Lii, J.-H.; Allinger, N. L. *J. Am. Chem. Soc.* **1989**, *111*, 8576–8582.
16. Lii, J.-H.; Ma, B.; Allinger, N. L. *J. Comput. Chem.* **1999**, *20*, 1593–1603.
17. Sparkes, H. A.; Raithby, P. R.; Clot, E.; Shields, G. P.; Chisholm, J. A.; Allen, F. H. *Cryst. Eng. Commun.* **2006**, *8*, 563–570.
18. Hermida-Ramón, J. M.; Rios, M. A. *J. Phys. Chem. A* **1998**, *102*, 10818–10827.
19. Allen, F. H. *Acta Crystallogr., Sect. B* **2002**, *58*, 380–388.
20. Jarosz, S.; Listkowski, A.; Lewandowski, B.; Ciunik, Z.; Brzuszkiewicz, A. *Tetrahedron* **2005**, *61*, 8485–8492.
21. Thibodeaux, D. P.; Johnson, G. P.; Stevens, E. D.; French, A. D. *Carbohydr. Res.* **2002**, *337*, 2301–2310.
22. Gress, M. E.; Jeffrey, G. A. *Acta Crsytallogr., Sect. B.* **1977**, *33*, 2490–2495.
23. Brown, G. M.; Levy, H. A. *Acta Crystallogr., Sect. B.* **1979**, *35*, 656–659.
24. Kouwijzer, M. L. C. E.; van Eijck, B. P.; Kooijman, H.; Kroon, J. *Acta Crystallogr., Sect B.* **1995**, *51*, 209–220.
25. Jones, P. G.; Sheldrick, G. M.; Kirby, A. J.; Glenn, R. *Z. Kristallogr., Kristallgeom., Kristallphys., Kristallchem.* **1982**, *161*, 237–243.
26. Jones, P. G.; Sheldrick, G. M.; Kirby, A. J.; Glenn, R. *Z. Kristallogr., Kristallgeom., Kristallphys., Kristallchem.* **1982**, *161*, 245–251.
27. French, A. D.; Johnson, G. P.; Kelterer, A.-M.; Csonka, G. *Tetrahedron: Asymmetry* **2005**, *16*, 577–586.
28. French, A. D.; Johnson, G. P.; Kelterer, A.-M.; Dowd, M. K.; Cramer, C. J. *Int. J. Quantum Chem.* **2001**, *84*, 416–425.
29. French, A. D.; Johnson, G. P. *Cellulose* **2004**, *11*, 5–22.
30. French, A. D.; Kelterer, A.-M.; Johnson, G. P.; Dowd, M. K.; Cramer, C. J. *J. Comput. Chem.* **2001**, *22*, 65–78.
31. Mendonca, S.; Johnson, G. P.; French, A. D.; Laine, R. A. *J. Phys. Chem. A* **2002**, *106*, 4115–4124.
32. French, A. D.; Kelterer, A.-M.; Cramer, C. J.; Johnson, G. P.; Dowd, M. K. *Carbohydr. Res.* **2000**, *326*, 305–322.
33. French, A. D.; Kelterer, A.-M.; Johnson, G. P.; Dowd, M. K.; Cramer, C. J. *J. Mol. Graph. Model.* **2000**, *18*, 95–107.
34. Rees, D. A. *Polysaccharide Shapes*; John Wiley: New York, 1977, pp 41–42.
35. Shimanouchi, T.; Mizushima, S.-I. *J. Chem. Phys.* **1955**, *33*, 707–711.
36. Takahashi, Y.; Nishikawa, S. *Macromolecules* **2003**, *36*, 8656–8661.
37. Ramakrishnan, C.; Ramachandran, G. N. *Biophys. J.* **1965**, *5*, 909–933.
38. Saenger, W.; Jacob, J.; Gessler, K.; Steiner, T.; Hoffmann, D.; Sanbe, H.; Koizumi, K.; Smith, S. M.; Takaha, T. *Chem. Rev.* **1998**, *98*, 1787–1802.
39. Gessler, K.; Usón, I.; Takaha, T.; Krauss, N.; Smith, S. M.; Okada, S.; Sheldrick, G. M.; Saenger, W. *Proc. Natl. Acad. Sci. U.S.A.* **1999**, *96*, 4246–4251.
40. Pangborn, W.; Langs, D.; Pérez, S. *Int. J. Biol. Macromol.* **1985**, *7*, 363–369.
41. Hinrichs, W.; Saenger, W. *J. Am. Chem. Soc.* **1990**, *112*, 2789–2796.
42. Taga, T.; Inagaki, E.; Fujimori, Y.; Nakamura, S. *Carbohydr. Res.* **1993**, *240*, 39–45.
43. Taga, T.; Inagaki, E.; Fujimori, Y.; Nakamura, S. *Carbohydr. Res.* **1994**, *251*, 203–212.
44. Tanaka, I.; Tanaka, N.; Ashida, T.; Kakudo, M. *Acta. Crystallogr., Sect. B.* **1976**, *32*, 155–160.
45. Jeffrey, G. A.; Huang, D.-B. *Carbohydr. Res.* **1991**, *222*, 47–55.
46. Tanase, T.; Onaka, T.; Nakagoshi, M.; Kinoshita, I.; Shibata, K.; Doe, M.; Fugi, J.; Yano, S. *Inorg. Chem.* **1999**, *38*, 3150–3159.
47. Takusagawa, F.; Jacobson, R. A. *Acta Crystallogr., Sect. B* **1978**, *34*, 213–218.
48. Schouten, A.; Kanters, J. A.; Kroon, J.; Looten, P.; Duflot, P.; Mathlouthi, M. *Carbohydr. Res.* **1999**, *322*, 274–278.
49. Chu, S. S. C.; Jeffrey, G. A. *Acta Crystallogr.* **1967**, *23*, 1038–1049.